Physics of Plasmas

Self-acceleration and energy channeling in the saturation of the ion-sound instability in a bounded plasma

Cite as: Phys. Plasmas **27**, 080702 (2020); https://doi.org/10.1063/5.0016440
Submitted: 05 June 2020 . Accepted: 03 August 2020 . Published Online: 21 August 2020

Liang Xu, Andrei Smolyakov, Salomon Janhunen, and Igor Kaganovich

Physics of Plasmas LETTER scitation.org/journal/php

Self-acceleration and energy channeling in the saturation of the ion-sound instability in a bounded plasma

Cite as: Phys. Plasmas **27**, 080702 (2020); doi: 10.1063/5.0016440
Submitted: 5 June 2020 · Accepted: 3 August 2020 ·
Published Online: 21 August 2020

Liang Xu,[1,2,a)] Andrei Smolyakov,[2] Salomon Janhunen,[2] and Igor Kaganovich[3]

AFFILIATIONS

[1]Institute for Theoretical Electrical Engineering, Ruhr University Bochum, D-44780 Bochum, Germany
[2]Department of Physics and Engineering Physics, University of Saskatchewan, Saskatoon, Saskatchewan S7N 5E2, Canada
[3]Plasma Physics Laboratory, Princeton University, Princeton, New Jersey 08543, USA

[a)]Author to whom correspondence should be addressed: Liang.Xu@ruhr-uni-bochum.de

ABSTRACT

A novel regime of the saturation of the Pierce-type ion-sound instability in a bounded ion-beam-plasma system is revealed in 1D particle-in-cell simulations. It is found that the saturation of the instability is mediated by the oscillating virtual anode potential structure. The periodically oscillating potential barrier separates the incoming beam ions into two groups. One component forms a supersonic beam, which is accelerated to an energy exceeding the energy of the initial cold ion beam. The other component is organized as a self-consistent phase space structure of trapped ions with a wide energy spread—the ion hole. The effective temperature (energy spread) of the ions trapped in the hole is lower than the initial beam energy. In the final stage, the ion hole expands over the whole system length.

Plasma physics has yielded many important results in the theory of nonlinear waves. Earlier theories of coherent nonlinear waves, shocks, and solitons[1] have been expanded to include nonlinear structures in phase space, such as Bernstein–Greene–Kruskal (BGK) states,[2] electron and ion holes,[3–9] and clumps.[10,11] Such structures have been identified as the nonlinear saturated states of the beam-like kinetic instabilities in collisionless and weakly collisional plasmas when the dynamics is dominated by a single coherent wave. The saturation mechanism via the formation of long lived phase space structures is a scenario alternative to the quasilinear saturation in the case of a wide spectrum of overlapping modes resulting due to the flattening of the distribution function. Phase space holes/clumps have been detected in space plasmas[11–15] and shown to be important for the saturation of fast particle driven instabilities in fusion plasmas.[10,16–19] Many numerical experiments[3,9,11,20–26] have demonstrated phase space structures as a result of the saturation of bump-on-tail and Buneman instabilities. Most analytical and numerical studies have dealt with periodic systems. In practical laboratory applications, however, plasmas are typically bounded by walls that introduce important constraints. In this Letter, we present a novel mechanism of the nonlinear saturation of the ion-sound instability in a bounded plasma penetrated by a cold ion beam.

In a warm infinite plasma, the ion-sound instability of kinetic nature[27,28] occurs when the current drift velocity exceeds the phase velocity of the ion sound waves $v_0 > c_s/(1 + k^2\lambda_{De}^2)^{1/2}$, where c_s is the ion sound velocity, λ_{De} is the Debye length, and k is the wave number. In a bounded plasma of finite length, there exists much stronger fluid instability of the Pierce type for $v_0 < c_s$, which has been studied theoretically[29–31] and has been observed in experiments.[29] The linear stage of the Pierce-type ion beam instability has been well studied theoretically. Experiments in double plasma devices have revealed complex dynamics of Pierce instabilities induced by the ion and electron beams. Nakamura *et al.*[29] have observed ion sound waves and nonlinear harmonics. The oscillations were experimentally identified by Matsukuma and Kawai.[32] In the electron-beam-plasma system, Iizuka *et al.*[33–35] have demonstrated large scale current oscillations, the virtual cathode trapping ions, and the double-layer formation.

In this Letter, we show that a strong ion sound instability induced by the ion flow in a bounded plasma saturates through the formation of the virtual anode potential structure that exhibits coherent large amplitude oscillations. The large amplitude periodic oscillations of this localized potential, on one hand, accelerate a fraction of the ion beam (initially subsonic) to supersonic velocity. On the other hand, the oscillating potential barrier stops a fraction of the ion beam, resulting in

the formation of a long-lived large scale ion hole with a negative potential and a large population of trapped ions. Thus, a fraction of the initial energy of the ion beam $m_i n_{i0} v_0^2/2$ with $v_0 < c_s$ is channeled to a higher energy creating a lower density supersonic beam with velocity $v_b > c_s$, while the rest of the beam energy is spread to lower energies forming the phase space vortex of trapped ions with a wide energy spread with an effective temperature $T_{tr} < m_i v_b^2/2$, where m_i is the ion mass and n_{i0} is the density of injected ions. In our case, $T_{tr} \simeq m_i v_b^2/6$.

A simplified 1D collisionless plasma model with a cold ion beam injected into the system is studied using the 1D3V electrostatic direct implicit particle-in-cell code (EDIPIC),[36] which has been comprehensively validated and benchmarked.[37,38] We focus only on the ion sound-type low frequency fluctuations $\omega/k \ll v_{th,e}$, where $v_{th,e}$ is the electron thermal velocity, so that Boltzmann-distributed electrons are used while the ions are computed kinetically. Specifically, the movement of ion superparticles is computed through integration of the Newtonian equations of motion, while the electron density is calculated as $n_e = n_{e0} \exp[e\varphi(x)/T_e]$ as required in the Poisson solver, where n_{e0} is the unperturbed electron density, $\varphi(x)$ is the electric potential at the previous time moment, and T_e is the electron temperature. In the Poisson solver, multiple iterations give the converged solution of $n_e(x)$ at the present moment and also the electric field and potential, which advance the ions and give the initial electron density for iteration at the next time moment.

In the simulations, the grounded walls are set at locations $x = 0$ and $x = d$, with the electric potential $\varphi(x = 0) = \varphi(x = d) = 0$. Ions with constant flux and velocity v_0 are injected from the left wall. The ions approaching the walls are absorbed. Initially, the electron density is set to be $n_{e0} = 10^{14}\,\mathrm{m}^{-3}$ and the (injected) ion density is slightly different to produce a charge perturbation with the value $\delta n = (n_{i0} - n_{e0})/n_{e0} \approx \pm 0.1\%$. In this Letter, positive initialization ($\delta n > 0$) was used, leading to the ion hole formation. For simplicity, the ion mass m_i is set to be 1 in atomic units. The Debye length in the simulations is calculated to be $\lambda_{De} = 1.3\,\mathrm{mm}$ and the simulation box length is set as $d = 50\lambda_{De}$ with the spatial resolution of $\Delta x = \lambda_{De}/10$. Therefore, the simulation domain constitutes 500 cells and $d = 6.5\,\mathrm{cm}$. The time step is chosen as $\Delta t = 1 \times 10^{-11}\,\mathrm{s}$ so that the ion dynamics is resolved with a high resolution. The high frequency mode damping in an implicit code can also be avoided because of the small time step.[39] Two thousand superparticles per cell are used. The dynamics time scale of the ion wave studied here is much slower than the time scale of the electron motion, and adiabatic electron assumption is, therefore, satisfied. In this paper, electron temperature $T_e = 3\,\mathrm{eV}$ is used throughout this work.

In the linear regime, when the kinetic effects of ion trapping are not important, our simulations recover the results of the analytical theory and the fluid simulations of the ion sound instability in a bounded plasma by Koshkarov *et al.*[31] This is shown in Figs. 1(a) and 1(b), which compare the growth rates and eigenmodes of the Pierce type ion sound instability obtained from our PIC simulations and the linear theory.[31] In the simulations of Figs. 1(a) and 1(b), the system length is $d = 10\lambda_{De}$. In Fig. 1(a), the growth rates as a function of the ion beam velocity in the range of $0.4c_s$–$1.0c_s$ are compared between our simulations and theory. In Fig. 1(b), the eigenmodes (including ion density, velocity, and potential) are also compared when the ion beam velocity is $0.86c_s$. The linear growth rates and eigenmodes obtained from the

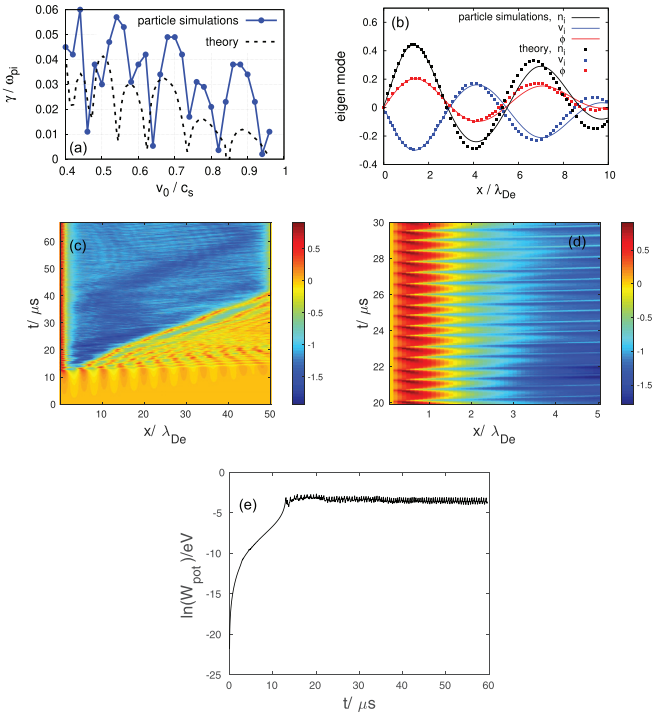

FIG. 1. (a) Linear growth rates and (b) linear eigenmodes of the ion sound instability from PIC simulations and fluid theory.[31] (c) Potential oscillations in linear and nonlinear regimes. The color bar shows the scale of potential. The ions are injected at the left wall ($x = 0$) and absorbed at the right wall ($x = d = 50\lambda_{De}$). (d) Coherent oscillations of the virtual anode potential structure [zoomed picture of (c) close to the left wall] in the nonlinear regime. (e) The evolution of the potential energy density as a function of time, showing the growth and saturation of the instability.

simulations and theory, Figs. 1(a) and 1(b), are in reasonable agreement, taking into account that the analytical theory is formulated for the asymptotic limit of finite but small wave numbers, $k\lambda_{De} \ll 1$, while in our simulations $k\lambda_{De} \simeq 1$, see Fig. 1(b). We note that according to the theory, the ion sound instability occurs only for $v_0 < c_s$, while the case $v_0 > c_s$ is stable for this type of instability.

As was shown analytically,[31] the instability occurs in the alternating oscillatory [real part of frequency $Re(\omega) \neq 0$] and aperiodic [$Re(\omega) = 0$] zones as the ion beam velocity changes. In our nonlinear simulations, Figs. 1(c)–1(e), the ion beam velocity is $v_0 = 0.8c_s$. With this value and $d = 50\lambda_{De}$, the instability occurs in the aperiodic zone, and so the fluctuations grow as a standing wave as it is clearly seen in Fig. 1(c) showing the spatial and temporal evolution of the potential. Figure 1(e) shows the time evolution of the normalized potential energy density $W_{pot} = 1/(n_{i0}d)\int_0^d 1/2\epsilon_0 E^2 dx$, from which the growth rate is calculated to be about $0.02\omega_{pi}$ in the linear stage, consistent with the fluid numerical calculation of the linear theory.

The linear growth and the transition to the nonlinear stage can be seen in the ion phase space plane, potential, and ion density profiles shown in Fig. 2 for different points in time. Initially, the potential is $\varphi(x) = 0$ with a mono-energetic ion flow throughout the simulation box. The absolute mode amplification starts at the left wall, as predicted by the linear theory. The exponential growth occurs after the

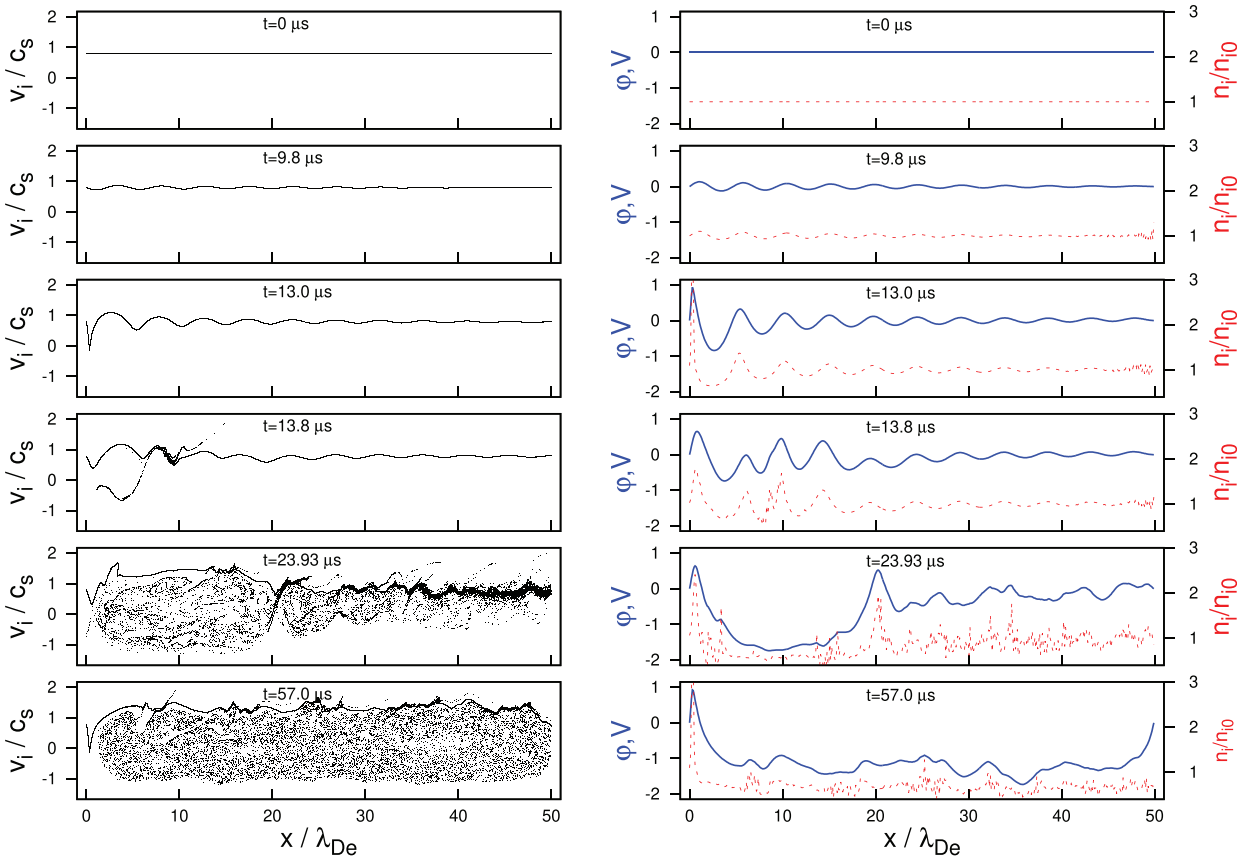

FIG. 2. The ion phase plane, potential, and ion density profiles at different times of the linear instability ($t < 13\,\mu$s), wave breaking forming multi-valued solutions ($t > 13.8\,\mu$s) to the large-scale ion hole of the system size in the final stage $t = 57\,\mu$s.

ion transit (over the box length) time, and the potential reaches 0.1 V near the left wall around 9.8 μs. The ion velocity is still single valued at this time, which suggests that the fluid description still holds. The transition from the linear regime to the nonlinear regime takes place when the wave amplitude reaches a critical level at which the ions are stopped by and trapped in the wave potential. With the cold ion beam, the critical wave potential threshold is $\varphi_{th} = 1/2 m_i v_0^2/e$, and accordingly, $\varphi_{th} = 0.96$ V when $v_0 = 0.8 c_s$. One can see from Fig. 2 that around $t \simeq 13.0\,\mu$s, the potential perturbation reaches the threshold value and forms a peaked structure (in the first half-wavelength) ending in the singularity and subsequent multi-valued solutions, seen at time $t = 13.8\,\mu$s in Fig. 2. Multi-valued solutions occur due to the ion reflection by the potential barrier structure, as illustrated in Fig. 2 ($t = 13.8\,\mu$s) by the appearance of the ions with negative velocities. The potential barrier near the left wall (called below as a virtual anode) oscillates in both time and space; the zoomed-in space-time profile of the potential near the left wall is shown in Fig. 1(d). The virtual anode oscillations are rather coherent in time with a frequency of the order ω_{pi} corresponding to the ion sound oscillations in the short wavelength regime, $k\lambda_{De} \gg 1$.

The periodically oscillating potential barrier (oscillating virtual anode) creates two related phenomena. In the raising stage, it accelerates the beam ions to a velocity larger than the velocity of the initial beam, i.e., $v_b > v_0$ (in this case, $v_0 = 0.8 c_s$). In fact, the fraction of the original beam ions is accelerated to supersonic velocities of the order of $1.3 c_s$, see Fig. 3. On the other hand, the large potential barrier breaks the flow of ions, decelerating and partially reflecting them. In

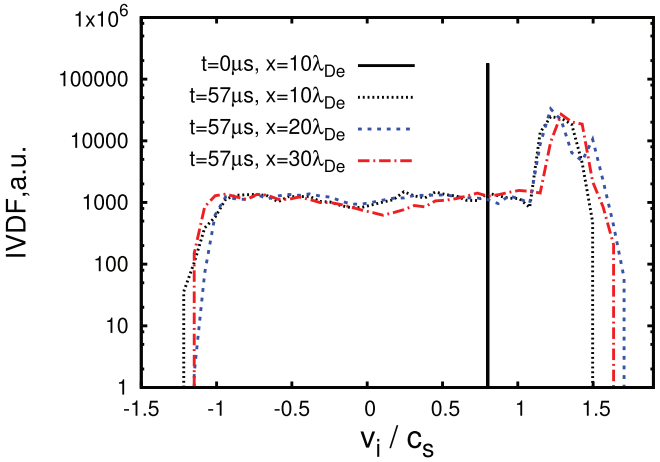

FIG. 3. The ion velocity distribution in the initial and final stages.

the decaying stage of the potential, some decelerated ions are released, forming the population of the trapped ions of a finite temperature, which results in the ion hole. The formation of the ion hole is clearly seen at $t = 23.93\,\mu$s, Fig. 2. The trapped ions have a finite temperature due to scattering from the periodically oscillating virtual anode. Therefore, the oscillating virtual anode structure results in the acceleration of some ions forming a supersonic beam with $v_b > c_s > v_0$ and the heating of other ions. In Fig. 3, this energy channeling is shown by the evolution of the ion velocity distribution from the delta function of the cold ions beam with $v_i = v_0 = 0.8c_s$ at $t = 0\,\mu$s to the wide distribution with a beam fraction of the order $v_i = v_b = 1.3c_s$ and the trapped ion population with a finite temperature (effective mean energy) $T_{tr} \simeq 0.8$ eV at $t = 57\,\mu$s. The trapped ions result in the ion hole with negative potential, which eventually expands through the whole system as shown in Fig. 2.

The ion trapping occurs in several stages as a result of consecutive decelerating and scattering events. Several of such events are shown in the ion phase plane, ion density, and potential profiles in one snapshot $t = 23.93\,\mu$s as shown in Fig. 4. One can see the localized bunches (labeled as 1, 2, and 3) of increased ion density at the locations of decreased ion velocity, which also correlate with the peaks in the potential. The most recent bunch of decelerated ions (the arrow 3 position) is shown around the virtual anode location near the left boundary. The bunch, which was released earlier, is scattered at the location marked by arrow 2. The earliest bunch in this snapshot is marked by arrow 1, where one can see the velocity depletion and strong density enhancement at the location of large potential peak. Effectively, this location corresponds to the ion hole boundary that moves toward the right wall. The velocity of the ion hole expansion is estimated here as the thermal (mean) velocity of trapped ions $\langle v_{tr} \rangle = \frac{1}{2} v_b$, and the temperature of the trapped ions is $T_{tr} = \frac{1}{6} m_i v_b^2$.

In the saturated stage, the fluctuation spectrum consists of the Doppler shifted ion sound modes and the nonlinear harmonics of the short wavelength ion sound $\omega = \omega_{pi}$ for $k\lambda_{De} \gg 1$, as illustrated in Fig. 5 for the Fourier transform of ion density over the whole space and in the time range of 45–70 μs. The two lines in Fig. 5 are the dispersion relations of Doppler-shifted ion sound waves,

$$\omega/\omega_{pi} = kv_b/\omega_{pi} \pm k\lambda_{De}\left[1 + (k\lambda_{De})^2\right]^{-1/2}. \quad (1)$$

The sign $\pm$ represents the two branches of the ion sound wave, fast beam mode and slow beam mode. As mentioned in Fig. 3, the beam velocity $v_b \approx 1.3c_s$. It is shown in Fig. 5 that the calculation by Eq. (1) agrees well with the simulation. In addition, one can identify the oscillations with ion plasma frequency and its multiple harmonics, which are the typical feature of the oscillating virtual anode,[40] also reminiscent of the experimental observations in Ref. 29.

It is proposed in this Letter that the described nonlinear structures due to the ion sound instability are a general phenomenon in bounded subsonic ion beam plasma systems. The instability is reactive, of the type of the negative energy instabilities, and occurs as a result of the coupling (mediated by plasma boundaries) of the ion sound waves propagating in opposite directions. A supersonic ion beam in the plasma with adiabatic electrons is stable and is not subject to the Pierce-type ion sound instability, which was also predicted by the linear theory.[31] The characteristics of the instability in our simulations, e.g., perturbations of the plasma density, and ion velocity are in accord with predictions of the linear theory: the instability type (aperiodic or oscillatory) and growth rates. The nonlinear scenario described in this Letter applies for both the oscillatory $[Re(\omega) \neq 0]$ and aperiodic instability zones $[Re(\omega) = 0]$ with one exception. For the aperiodic instability with negative density initialization $\delta n < 0$, a different type of coherent structure develops in the nonlinear phase. This asymmetry is related to the preference (from the thermodynamic perspective) for the ion hole formation and will be addressed in a separate study.

In summary, we report a novel mechanism of trapped ion phase space hole formation in a bounded ion-beam-plasma system driven by the Pierce-type ion sound instability due to the presence of boundaries. Our simulations agree well with the linear theory of such an instability. In the nonlinear stage, we observe an oscillating potential barrier structure (i.e., the virtual anode) splitting the ion beam and channeling

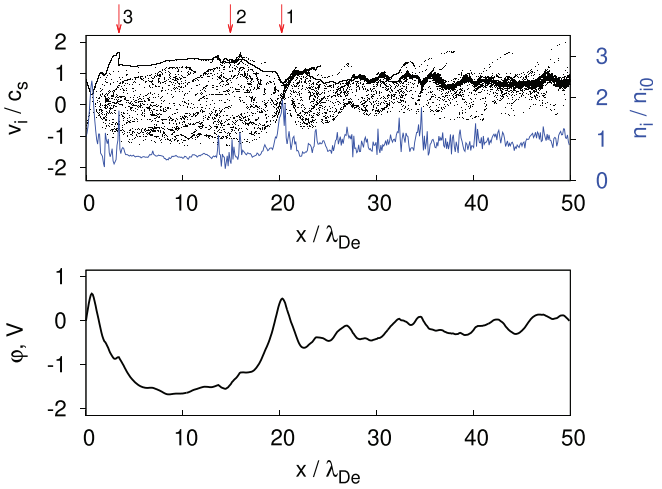

FIG. 4. Several decelerating/scattering events with enhanced density bunches (labeled as 1, 2, and 3) are shown in the ion phase space plane, ion density, and potential profile at the snapshot $t = 23.93\,\mu$s.

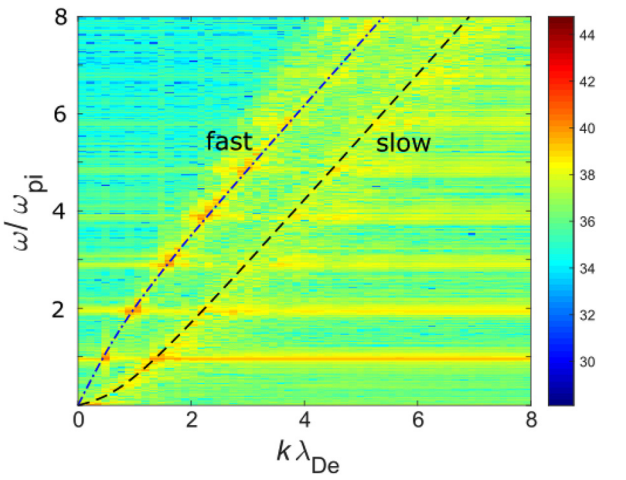

FIG. 5. A Fourier transform of the ion density over the whole simulation box and in the time range 45–70 μs shows the spectra of fluctuations. The two lines are the theoretical prediction given by Eq. (1).

energy to a population of the higher energy ions while heating the ions at lower energies. The higher energy fraction of accelerated ions forms the supersonic ion beam, while the group of decelerated ions forms a system-long ion hole of trapped ions.

We note that the simulations with the warm ion flow of different ion temperatures were carried out and also verified the results described in this Letter. Please refer to the animation[41] showing the ion phase plane with warm ions ($T_i = 0.03$ eV) flowing through the bounded system. It would be of great interest to validate our simulations and theory in experiments so that the non-1D effect and collision effect can be further investigated. Like the experimental setup in the work,[29,42] it is suggested that the widely used double plasma device is able to generate the desired subsonic ion beam in the source chamber and expected to reproduce the wave-particle-boundary (grids) interactions in the target chamber. It is noteworthy that only an electron emitter should be used instead of the plasma generator in the target chamber in order to avoid the presence of background ions.

A similar nonlinear phenomenon presented in this work can be expected in material processing (atomic layer etching/deposition) devices[43,44] with low energy ions, as well as Hall plasmas,[30] Q machines,[45] and inertial confinement fusion drivers[46–48] when ion beam Pierce instability[30,49] is excited.

This work was supported in part by NSERC Canada and the Air Force Office of Scientific Research No. FA9550-15-1-0226. Computational resources were provided by ComputeCanada/WestGrid. The authors would like to express their gratitude to Professor Brinkmann, Edward Startsev, and Jian Chen for insightful discussions and suggestions.

DATA AVAILABILITY

The data that support the findings of this study are available from the corresponding author upon reasonable request.

REFERENCES

[1]R. Z. Sagdeev and A. A. Galeev, *Nonlinear Plasma Theory* (Benjamin, New York, 1969).
[2]I. B. Bernstein, J. M. Greene, and M. D. Kruskal, Phys. Rev. **108**, 546 (1957).
[3]K. Roberts and H. L. Berk, Phys. Rev. Lett. **19**, 297 (1967).
[4]H. Pécseli, R. Armstrong, and J. Trulsen, Phys. Lett. A **81**, 386 (1981).
[5]H. Schamel, Phys. Rep. **140**, 161 (1986).
[6]B. Eliasson and P. Shukla, Phys. Rep. **422**, 225 (2006).
[7]A. Kabantsev, J. Yu, R. Lynch, and C. Driscoll, Phys. Plasmas **10**, 1628 (2003).
[8]A. Hasegawa and T. Sato, Phys. Fluids **25**, 632 (1982).
[9]H. L. Pécseli, J. Trulsen, and R. J. Armstrong, Phys. Scr. **29**, 241 (1984).
[10]H. L. Berk, B. N. Breizman, and M. Pekker, Phys. Rev. Lett. **76**, 1256 (1996).
[11]H. L. Berk, B. N. Breizman, and N. V. Petviashvili, Phys. Lett. A **234**, 213 (1997).
[12]R. Ergun, Y.-J. Su, L. Andersson, C. Carlson, J. McFadden, F. Mozer, D. Newman, M. Goldman, and R. Strangeway, Phys. Rev. Lett. **87**, 045003 (2001).
[13]M. Temerin, K. Cerny, W. Lotko, and F. Mozer, Phys. Rev. Lett. **48**, 1175 (1982).
[14]R. Boström, G. Gustafsson, B. Holback, G. Holmgren, H. Koskinen, and P. Kintner, Phys. Rev. Lett. **61**, 82 (1988).
[15]C. Cattell, J. Dombeck, J. Wygant, J. Drake, M. Swisdak, M. Goldstein, W. Keith, A. Fazakerley, M. André, E. Lucek *et al.*, J. Geophys. Res. **110**, 1201, https://doi.org/10.1029/2004JA010519 (2005).
[16]K. Miyamoto, *Translation* (MIT Press, Cambridge, Mass, 1980), p. 625.
[17]M. C. Herrmann and N. J. Fisch, Phys. Rev. Lett. **79**, 1495 (1997).
[18]F. Zonca, L. Chen, S. Briguglio, G. Fogaccia, A. V. Milovanov, Z. Qiu, G. Vlad, and X. Wang, Plasma Phys. Controlled Fusion **57**, 014024 (2015).
[19]L. Chen and F. Zonca, Rev. Mod. Phys. **88**, 015008 (2016).
[20]I. H. Hutchinson, Phys. Plasmas **24**, 055601 (2017).
[21]D. L. Newman, M. V. Goldman, M. Spector, and F. Perez, Phys. Rev. Lett. **86**, 1239 (2001).
[22]M. Medvedev, P. Diamond, M. Rosenbluth, and V. Shevchenko, Phys. Rev. Lett. **81**, 5824 (1998).
[23]F. Valentini, F. Califano, D. Perrone, F. Pegoraro, and P. Veltri, Phys. Rev. Lett. **106**, 165002 (2011).
[24]C. Lan and I. D. Kaganovich, preprint arXiv:1909.09281 (2019).
[25]K. Hara and C. Treece, Plasma Sources Sci. Technol. **28**, 055013 (2019).
[26]C. Zhou and I. Hutchinson, Phys. Plasmas **23**, 082102 (2016).
[27]A. Galeev and R. Sagdeev, *Reviews of Plasma Physics*, edited by M. A. Leontovich (Consultants Bureau, New York, 1979), p. 257.
[28]J. Wesson, A. Sykes, and H. Lewis, Plasma Phys. **15**, 49 (1973).
[29]S. Nakamura, T. Yuyama, M. Takeyama, and H. Kubo, J. Phys. Soc. Jpn. **51**, 3006 (1982).
[30]A. Kapulkin and E. Behar, IEEE Trans. Plasma Sci. **43**, 64 (2015).
[31]O. Koshkarov, A. I. Smolyakov, I. D. Kaganovich, and V. I. Ilgisonis, Phys. Plasmas **22**, 052113 (2015).
[32]M. Matsukuma and Y. Kawai, J. Phys. Soc. Jpn. **70**, 3560 (2001).
[33]S. Iizuka, K. Saeki, N. Sato, and Y. Hatta, Phys. Rev. Lett. **43**, 1404 (1979).
[34]S. Iizuka, K. Saeki, N. Sato, and Y. Hatta, J. Phys. Soc. Jpn. **54**, 146 (1985).
[35]S. Iizuka, K. Saeki, N. Sato, and Y. Hatta, J. Phys. Soc. Jpn. **54**, 950 (1985).
[36]D. Sydorenko, "Particle-in-cell simulations of electron dynamics in low pressure discharges with magnetic fields," Ph.D. thesis (University of Saskatchewan, Saskatoon, 2006).
[37]J. Carlsson, A. Khrabrov, I. Kaganovich, T. Sommerer, and D. Keating, Plasma Sources Sci. Technol. **26**, 014003 (2016).
[38]L. Xu, A. V. Khrabrov, I. D. Kaganovich, and T. J. Sommerer, Phys. Plasmas **24**, 093511 (2017).
[39]A. Friedman, J. Comput. Phys. **90**, 292 (1990).
[40]A. Piel, H. Klostermann, A. Rohde, N. Jelić, and R. Schrittwieser, Phys. Lett. A **216**, 296 (1996).
[41]See https://youtu.be/AYyXBnlGJAU for animation of the ion phase plane evolution of an warm ion flow in a bounded plasma.
[42]S. Iizuka, K. Saeki, N. Sato, and Y. Hatta, J. Phys. Soc. Jpn. **52**, 1618 (1983).
[43]L. Xu, A. Nasrullah, Z. Chen, M. Jain, P. Ruchhoeft, D. J. Economou, and V. M. Donnelly, Appl. Phys. Lett. **92**, 013124 (2008).
[44]Y.-M. Chen, R. Sawadichai, S. Tian, V. M. Donnelly, P. Ruchhoeft, and D. J. Economou, J. Phys. D: Appl. Phys. **52**, 355205 (2019).
[45]S. Kuhn, Phys. Fluids **27**, 1834 (1984).
[46]J. Poukey, J. Quintenz, and C. Olson, Appl. Phys. Lett. **38**, 20 (1981).
[47]D. S. Lemons and J. R. Cary, J. Appl. Phys. **53**, 4093 (1982).
[48]H. Schamel and V. Maslov, Phys. Rev. Lett. **70**, 1105 (1993).
[49]O. Koshkarov, A. I. Smolyakov, A. Kapulkin, Y. Raitses, and I. Kaganovich, Phys. Plasmas **25**, 061209 (2018).